MRS Communications

https://doi.org/10.1557/s43579-022-00166-9

MRS Communications

Research Letter

A conductive AFM study of carbon-rich hexagonal (BN)C semiconductor alloys

N. Khan, Georgia Gwinnett College, School of Science and Technology, Lawrenceville, GA 30043, USA
M. R. Uddin, J. Li, J. Y. Lin, and H. X. Jiang, Department of Electrical and Computer Engineering, Texas Tech University, Lubbock, TX 79409, USA
Address all correspondence to N. Khan at **nkhan3@ggc.edu**

(Received 5 December 2021; accepted 22 February 2022)

Abstract

The conductive atomic force microscopy was employed to map different phases and their boundaries to provide insights into phase separation mechanisms in carbon-rich h-(BN)C alloys. One of three phases identified, had the highest average current of about 0.85 μA, second with no current (0 μA), and a third phase with an average current of about 0.3 μA, corresponding to the pure graphite (h-C), pure (h-BN) and the h-(BN)C random alloy phases, respectively. Two other phases, with an average current of about 0.15 μA and 0.6 μA, were identified to be most likely the boundaries between phases and alloys.

Introduction

Hexagonal boron nitride (h-BN), a two-dimensional (2D) layered van der Waals material with a bandgap energy of about 6 eV, have attracted a significant attention due to its high thermal conductivity, dielectric properties, inertness, and chemical stability.[1–6] These properties make h-BN an emerging material for applications in deep UV optoelectronic devices and high-temperature/power electronic devices.[7–9] The similarities in melting points and 2D layered crystalline structure with a small lattice mismatch of 1.7% between graphite (h-C) and h-BN provides the potential to synthesize h-$(BN)_{1-x}(C_2)_x$ alloys with a tunable bandgap from 0 to 6 eV.[4,10,11] Moreover, if successfully synthesized, the h-$(BN)_{1-x}(C_2)_x$ alloy system also allows the conductivity control from insulating semiconductor (undoped h-BN) to semi-metal (graphite), covering a spectrum range from deep ultraviolet to far infrared. On the carbon-rich side, h-$(BN)_{1-x}(C_2)_x$ alloys could also resolve the issue of 0 eV bandgap in graphene, as it allows the bandgap opening of graphite through alloying with h-BN. This alloy system is considered a promising candidate not only for electronic and optoelectronic devices, but also for applications in area such as high energy–density supercapacitors, enhanced performance in lithium batteries, and water purification, etc.[12–15] However, the phase stability of this alloy system would be critical for the design of such applications.

In synthesizing a semiconductor alloy material system, the differences in the lattice constants, growth temperatures and bond energies between constituents could cause phase separation and thereby prevent the realization of homogeneous alloys. For the (BN)C alloys, numerous experimental and theoretical studies have been conducted to understand the origins of phase separation.[16–21] The phase stability for monolayer (BN)C alloys has been investigated,[22–24] and their theoretical studies concluded that growth of (BN)C alloys is challenging due to the differences in bond energies between the constituent atoms. The structure including, B–N and C–C bonds are energetically favorable, because of the large bond energies of 4.0 eV and 3.71 eV respectively, whereas other bonds, i.e., C–N (2.83 eV), B–C (2.59 eV), B–B (2.32 eV) and N–N (2.11 eV) are less favorable. The large differences in bond energies tend to cause phase separation in h-$(BN)_{1-x}(C_2)_x$ alloy in the middle range of x.[17] The phase diagram was calculated for the cubic structured (BN)C alloy system, which showed that the miscibility could be overcome at high growth temperatures T ~ 3500 K, which is below the linear average of the melting points of h-BN and graphite.[23] However, there were also simulation results suggesting the possibility for obtaining homogenous (BN)C alloys with BN and carbon concentration of about 50%.[20,25,26] Previous experimental studies revealed that h-$(BN)_{1-x}(C_2)_x$ epilayers with $x \leq 0.95$ are most likely phase separated at a growth temperature of 1300°C.[16] However, detailed information regarding (i) the nature of phases that are involved in the phase separation, (ii) the structure of each phase, (iii) the boundaries between different phases, and (iv) the sizes and densities of phases are still lacking. The focus of this work is to answer above mentioned questions.

In this study, conductive atomic force microscopy (C-AFM) was employed to investigate the phase structures of high electrical conductive carbon-rich h-$(BN)_{1-x}(C_2)_x$ epilayers grown on c-sapphire substrates by metal organic chemical vapor deposition (MOCVD) at a growth temperature of 1300°C. In contrast to AFM, the C-AFM uses a conductive tip that scans across the surface, when a voltage is applied between tip and sample. Thus, the sample's topography and current mapping is measured simultaneously, enabling the direct correlation of a sample location with its electrical properties. Since h-C is a

semi-metal and h-BN is highly resistive with a measured electrical resistivity as larger as 10^{14} Ω cm,[27] the color contrast seen in C-AFM images provides the differences in electrical conductivities, which directly correlates with different phases (h-C, h-BN or h-(BN)C) and their boundaries in carbon-rich h-(BN)C alloy.

Experiment

The epitaxial layers of carbon-rich h-$(BN)_{1-x}(C_2)_x$ were synthesized on c-sapphire substrates using triethyl boron (TEB), ammonia (NH_3) and propane (C_3H_8) as the boron, nitrogen and carbon precursors, respectively. The supporting information (Fig. S1a) shows the schematic diagram of epilayer structure. A buffer layer of about 20 nm in thickness was first grown on the sapphire followed by an epilayer of h-BN with a thickness of 5 nm. The carbon-rich h-$(BN)_{1-x}(C_2)_x$ alloys with a thickness of 30 nm was then deposited on h-BN epilayer. Figure S1b shows an optical image of the top surface of an h-(BN)C epilayer grown on h-BN/sapphire template. The alloy samples were grown at 1300 °C using nitrogen as a carrier gas. A flow rate of 4.5 standard liter per minute (SLM) was used for NH_3, whereas the TEB and C_3H_8 flow rates were kept at 0.18 and 3.0 standard cubic centimeters per minute (sccm), respectively. Atomic composition results obtained from x-ray photoelectron spectroscopy (XPS) measurements revealed the atomic percentage of carbon of about 93% in C-rich h-$(BN)_{1-x}(C_2)_x$ alloy. The topography and local surface electrical conductivity were investigated using Multimode 8, AFM from Bruker, USA. The C-AFM was operated in contact mode to investigate phase structure of layers through the measurements of electrical current variations while simultaneously collecting topographic information.

Results and discussions

The 2D and 3D AFM images scanned across an (1 × 1) μm^2 scale are displayed in Fig. 1(a) and (b), which showed that the surface consists of bumps and valleys with a root mean square (RMS) roughness of about 6.4 nm. The 2D and 3D C-AFM images are shown in Fig. 1(c) and (d).

The color contrast seen in C-AFM [Fig. 1(c) and (d)] is caused by the differences in the electrical conductivities and hence represents different phases in h-(BN)C alloy. The black color region showed no conductivity. The blue, blue-green, green-red, and the red colors were representing different conductivities each. The red-color phase seemed to exist on its own, and around the edges of other phases, whereas blue-green, and green-red phases were coupled together. The zoomed in 2D C-AFM images on a (500 × 500) nm^2 area is shown in Fig. 1(e), and the graph for the current profiles along the line 1, 2, 3, and 4 is displayed in Fig. 1(f). The blue phase indicated in profile 1 of Fig. 1(e) has the highest current of about 0.8 μA and drops to 0 μA when the line extends in the black region as shown in Fig. 1(f). Based on the facts that h-BN is highly resistive and h-C is highly conductive, the black region with no current is the (h-BN) phase, and the blue region (profile 1) with the highest current is the graphite (h-C) phase.

The blue-green, and green-red phases indicated by profiles 2 and 3 of Fig. 1(e), have currents of about 0.6 μA and 0.35 μA, respectively as shown in Fig. 1(f). The red phase indicated through profile 4 has a lowest current of about 0.12 μA. The green-red (profile 3) should be representative of h-(BN)C alloys. The blue-green (profile 2), and the red (profile 4) should be the boundaries between (h-C) and h-(BN) C alloy, and (h-BN) and h-(BN)C alloys respectively.

Figure 2(a) shows the zoomed in C-AFM mapping at (200 × 200) nm^2, and the current profile along line 1 is shown in Fig. 2(b). The profile 1 in graph [Fig. 2(b)] showed the current mapping of different phases. Along the profile 1, in the C-AFM, the blue region in Fig. 2 showed the highest current of about 0.9 μA, and dropped to 0.6 μA when the blue–green region was mapped.

The current drops to 0 μA as the line was extended in the black region, and then rises again to about 0.6 μA when the blue-green region was mapped. The next region in C-AFM along profile 1 was red-colored, which showed the lowest current of about 0.15 μA. The last region mapped along the profile 1 was red-green region that showed a current of about 0.3 μA.

Figure 2(c) shows the current along profile 2, in the C-AFM image which showed almost the same current ranges as profile 1. Along the profile 2, in the C-AFM image, the blue region showed the current of about 0.98 μA, and dropped to 0 μA as the line was extended in the black region, and then rose again to about 0.65 μA when the blue-green region was mapped. The next region along profile 2 showed a current of about 0.30 μA when the green-red region was mapped. The results of current mapping along profile 1 and 2 are consistent with results from Fig. 1(e) and (f), as well as for different positions. The table in Fig. 2(c) summarizes the current ranges for different types of phases and boundaries for ten different scans.

The C-AFM results concluded that.

(i) Black phase with no current is the h-BN phase.
(ii) Green-red phase that showed an average of 0.30 μA is representative of h-(BN)C alloy. Thus, the red phase with an average current 0.15 μA ought to be the boundary between h-(BN)C alloy and h-BN.
(iii) Blue phase (h-C) possessed the highest average current of 0.85 μA. It is coupled with only the green phase. Thus, the blue-green phase with an average current 0.6 μA is mostly likely the boundary between h-C and h-(BN)C alloy.

The formation of different phases and their coupling could be explained from a bond energy perspective between different bonds. The black phase that is the (h-BN) phase is highly resistive and has a high bond energy (4.0 eV). The blue phase that is (h-C) phase is highly conductive, corresponding to a high bond

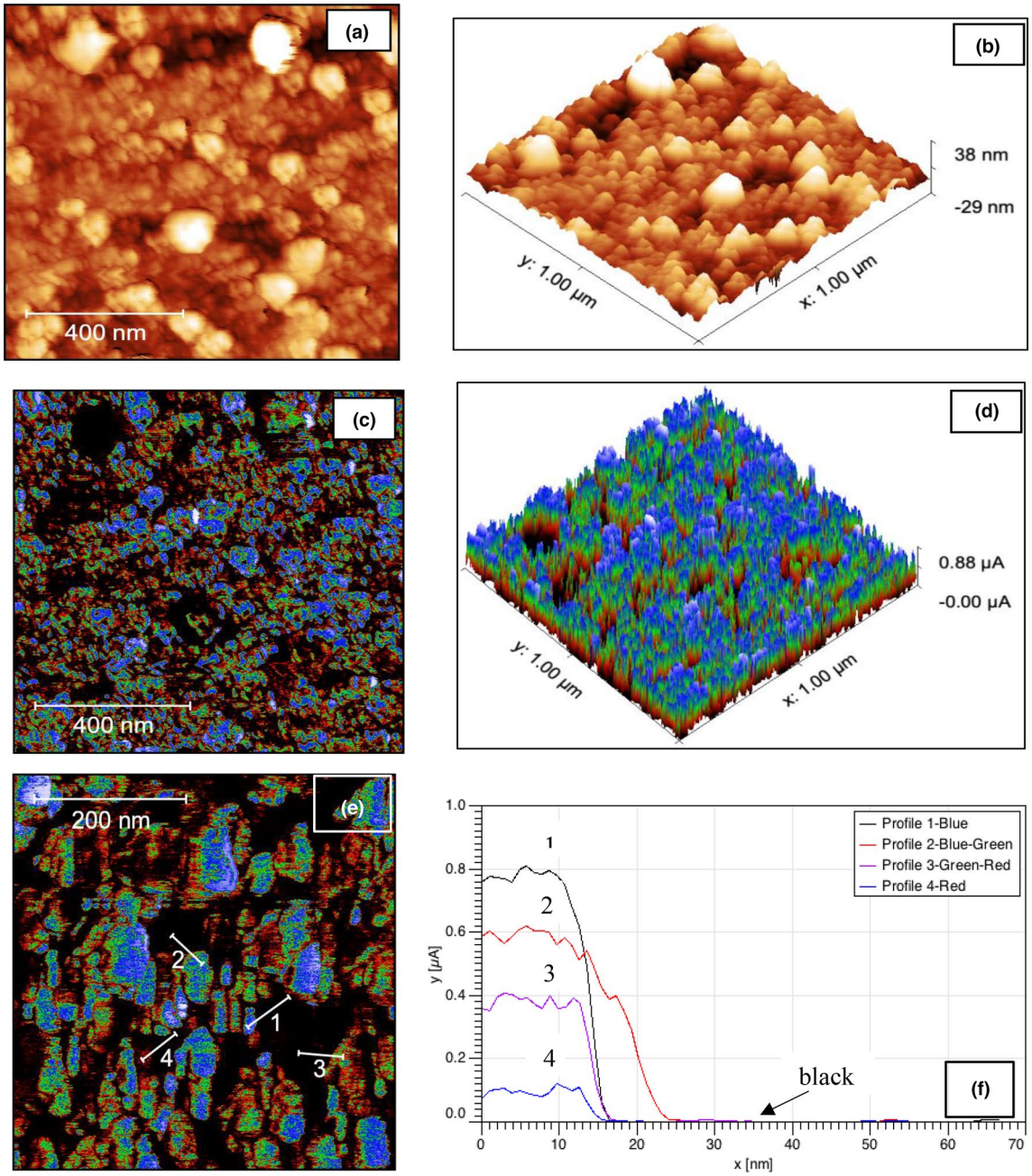

Figure 1. (a) 2D AFM image at (1 × 1) µm^2, (b) 3D AFM image at (1 × 1) µm^2, (c) 2D AFM image at (1 × 1) µm^2, (d) 3D C-AFM image at (1 × 1) µm^2, (e) 2D C-AFM image at (500 × 500) nm^2, and (f) graph showing current along profiles, 1, 2, 3 and 4 in Fig. 1(e).

energy as well (3.71 eV). The green-red phase is most likely the h-(BN)C random alloy phase. The boundaries between other phases probably represent a gradual change from one phase to another, to attain the lowest state of energy for the system. The total bond energy of all the bonds in h-(BN)C alloys is expected to be smaller than the sum of separated phases. For separated phases, due to the largest bond energies of (C–C) and (B–N) bonds, their number will be increased in comparison with that of random alloy, whereas the total number of (B–C) and (N–C) bonds with the bond energies of 2.59 eV and 2.83 eV, respectively, will be decreased in comparison to that of random alloys. However, since the total bond energies of (C–C) and (B–N) bonds are larger than those of (B–C) and (N–C) bonds and the total bond energy of h-(BN)C alloy system tends to be smaller than that of separated phases, the system ends up with phase separation when the carbon concentration is smaller than a certain value in carbon-rich h-(BN)C alloys.

The Fig. 3(a) shows the C_AFM image with boxes showing the approximate shape of the phases. The size for different phases seems to be irregular. However, mostly one side was

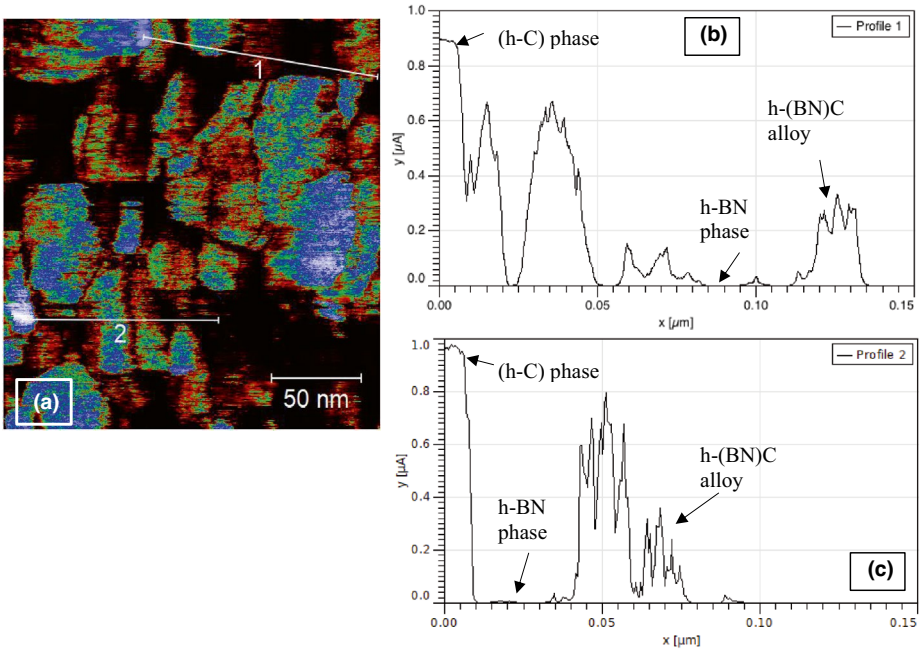

(d)

	C-AFM Color Contrast	Average Current (μA)	Type of Phases
1	Blue	0.85	h-C
2	Blue-Green	0.6	Boundary between (h-C) and h-(BN)C alloy
3	Green-Red	0.3	h-(BN)C alloy
4	Red	0.15	Boundary between (h-BN) and h-(BN)C alloy
5	Black	0	h-BN

Figure 2. (a) C-AFM image on a scale of (200 × 200) nm^2, (b) graph of current mapping along profile 1, (c) graph of current mapping along profile 2, and (d) table listing the current ranges for different types of phases observed by C-AFM.

larger than the other, except (h-BN) phase. The table in Fig. 3(b) summarized the data for the sizes of different phases for blue, blue-green, green-red, and red phases, which was collected at 10 different positions for each phase. The (h-BN) phase was black in color with zero conductivity. The blue phase (h-C) length and width were (40 ± 17) nm and (23 ± 8) nm, respectively, and had an area of (920 ± 711) nm^2, whereas length and width of blue-green phase [boundary between (h-C) and h-(BN)C alloy] were (45 ± 12) nm and (26 ± 8) nm, respectively, and had an area of (1170 ± 672) nm^2. The red-green phase [h-(BN)C alloy] length and width were (41 ± 10) nm and (23 ± 6) nm color region, respectively, and an area of (943 ± 476) nm^2. The length and width of red [boundary between (h-BN) and h-(BN)C alloy] were (16 ± 1) nm and (13 ± 3) nm, respectively, and had an area of about (208 ± 61) nm^2.

Red phase was smallest in size and mostly difficult to distinguish in term of shape as compared to others, as the region seemed to be fade and like dots or lines when existed on its own. The size of blue, blue-green and green-red phases seem to be close to each other. This could be due to these phases coupled together and couldn't be separated, although blue-green region had slightly larger area as compared to others.

In order to determine the percentage area covered by different phases and their boundaries as compared to h-BN, we conducted bearing analysis on C-AFM images, using data processing software "nasoscope analysis". The bearing analysis is used to determine what percentage of the surface lies above or below any arbitrarily chosen height. In our case bearing analysis was conducted to determine bearing percentage area above the threshold (bearing depth) of zero current. The

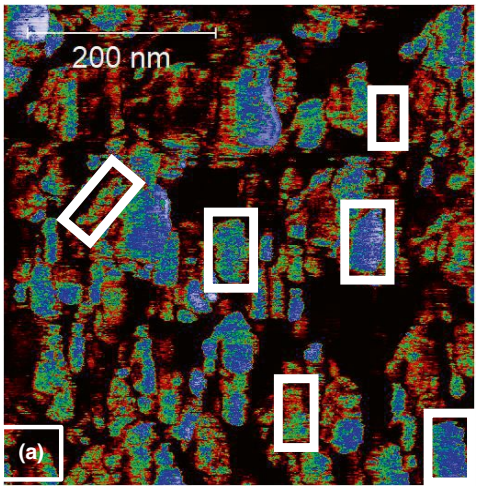

(b)	Blue-Region (h-C) phase 0.85 μA	Blue-Green Boundary 0.6 μA	Green-Red h-(BN)C alloy 0.3 μA	Red Boundary 0.15 μA	Black (h-BN) phase 0 μA
Length (nm)	40±17	45±12	41±10	16±1	No particular size
Width (nm)	23±8	26±8	23±6	13±3	No particular size
Area $(nm)^2$	920±711	1170±672	943±476	208±61	No particular size

Figure 3. (a) C-AFM image with boxes indicating the shape of phases, and (b) table listing the sizes of different phases.

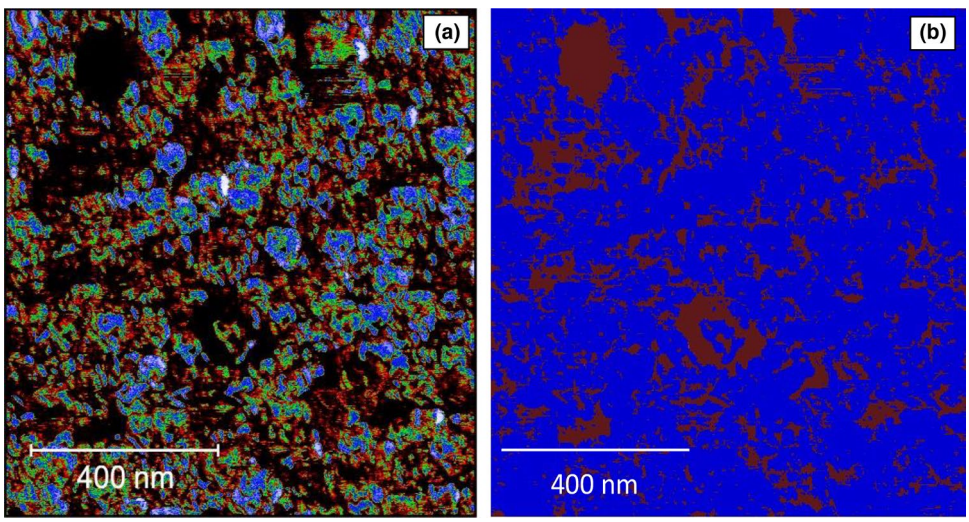

Figure 4. (a) C-AFM image at (1 × 1) m^2 scale, (b) corresponding bearing analysis images.

analysis provided information on the percentage area covered by different phases and their boundaries as compared to h-BN. The bearing percentage area for a bearing depth of zero current varied from about 60 to 80%. Figure 4 shows an example of the C-AFM image (Fig. 4a), and the corresponding bearing analysis image (Fig. 4b) which indicated the bearing area of about 78% (blue color) for a bearing depth of zero current, which meant that different phases and their boundaries in carbon-rich h-$(BN)_{1-x}(C_2)_x$ with ($x \sim 0.93$) alloy covered 78% of the area as compared to h-BN (Fig. 4).

Conclusions

In this study, C-AFM was employed to probe the phase separation in carbon-rich h-$(BN)_{1-x}(C)_x$ epilayers grown by MOCVD. The C-AFM directly mapped differences in electrical conductivities in different regions, and hence the phase separation in carbon-rich h-$(BN)_{1-x}(C)_x$ alloys provided insights into phase separation mechanism in h-(BN)C alloys. The boundaries between different phases might change gradually from one phase to another to achieve the lowest state of energy for the system. Three phases, including one with the highest average current of about 0.85 μA, another with no current (0 μA) and a third with an average current of 0.3 μA, corresponding respectively to the pure graphite (h-C), pure (h-BN) and h-(BN)C random alloy phases, were identified. Two other phases, a red-colored phase with an average current of about 0.15 μA and another blue-green colored phase with an average current of 0.6 μA, were identified to be most likely associated with the boundaries between h-BN/h-(BN)C alloys and (h-C)/h-(BN)C alloy, respectively. Future work would include using C-AFM to investigate, (i) Phase separation mechanism in boron rich h-(BN) C alloys, (ii) Study the effects of different growth conditions such as growth temperature, growth rate, III/V ratio, etc. on both carbon and boron rich h-(BN) C alloys, (iii) How the different phases evolve with thickness of epilayers in both carbon and boron rich h-(BN) C alloys.

Acknowledgments

The work at Georgia Gwinnett College was supported by National Science Foundation award CHE –1621665. The work at Texas Tech University is supported by DOE ARPA-E (DE-AR0001257).

Data availability

The data presented in this study are available on request from the corresponding author.

Declarations

Conflict of interest

The authors have no conflict of interest to declare that are relevant to the content of this article.

Supplementary Information

The online version contains supplementary material available at https://doi.org/10.1557/s43579-022-00166-9.

References

1. G. Cassabois, P. Valvin, B. Gil, Nat. Photonics **10**, 262–268 (2016)
2. R. Decker, Y. Wang, V.W. Brar, W. Regan, H. Tsai, Q. Wu, W. Gannett, A. Zettl, M.F. Crommie, Nano Lett. **11**, 2291–2295 (2011)
3. L. Song, L. Ci, H. Lu, P.B. Sorokin, C. Jin, J. Ni, A.G. Kvashnin, D.G. Kvashnin, Lou, B.I. Yakobson, P.M. Ajayan, Nano Lett. **10**, 3209 (2010)
4. C.R. Dean, A.F. Young, I. Meric, C. Lee, L. Wang, S. Sorgenfrei, K. Watanabe, T. Taniguchi, P. Kim, K.L. Shepard, J. Hone, Nature Nanotechnol. **5**, 722 (2010)
5. R.Y. Tay, M.H. Griep, G. Mallick, S.H. Tsang, R.S. Singh, T. Tumlin, E.H.T. Teo, S.P. Karna, Nano Lett. **14**(2), 839–846 (2014)
6. A. Lipp, K.A. Schwetz, K. Hunold, J. Eur. Ceram. Soc **5**, 3–9 (1989)
7. S. Majety, J. Li, X. K. Cao, R. Dahal, B. N. Pantha, J. Y. Lin, H. X. Jiang, Appl. Phys. Lett. 100, 061121 (2012) and *ibid* Proc. SPIE 8268, 82682R (2012).
8. Y. Kubota, K. Watanabe, O. Tsuda, T. Taniguchi, Sci. **317**, 932 (2007)
9. M. Šiškins, C. Mullan, S. Son, J. Yin, K. Watanabe, T. Taniguchi, D. Ghazaryan, K.S. Novoselov, A. Mishchenko, Appl. Phys. Lett. **114**, 123104 (2019)
10. S.K. Jang, J. Youn, Y.J. Song, S. Lee, Sci. Rep. **6**, 30449 (2016)
11. Y. Koretaka, Phys. Rev. B **79**, 144109 (2009)
12. L. Liao, K. Liu, W. Wang, X. Bai, E.G. Wang, Y. Liu, J. Li, C. Liu, J. Am. Chem. Soc. **129**(31), 9562–9563 (2007)
13. S. Wang, F. Ma, H. Jiang, Y. Shao, Y. Wu, X. Hao, A.C.S. Appl, Mater. Interfaces **10**(23), 19588–19597 (2018)
14. W. Lei, S. Qin, D. Liu, D. Portehault, Z. Liu, Y.I. Chen, Chem. Commun. **49**(4), 352–354 (2013)
15. Y. Guo, C. Yan, P. Wang, L. Rao, C. Wang, Chem. Eng. Sci. **387**, 124136 (2020)
16. M.R. Uddin, J. Li, J.Y. Lin, H.X. Jiang, J. Appl. Phys. **117**, 215703 (2015)
17. M.R. Uddin, S. Majety, J. Li, J.Y. Lin, H.X. Jiang, J. Appl. Phys. **115**, 093509 (2014)
18. J. Lu, K. Zhang, X.F. Liu, H. Zhang, T.C. Sum, A.H. Castro Neto, K.P. Loh, Nat. Commun. **4**, 2681 (2013)
19. K. Yuge, A. Seko, Y. Koyama, F. Oba, I. Tanaka, Phys. Rev. B **77**, 094121 (2008)
20. A. Jamr'oz, J.A. Majewski, Phys. Status Solidi B Basic Res. **256**, 1800554 (2019)
21. L. Ci, L. Song, C. Jin, D. Jariwala, D. Wu, Y. Li, A. Srivastava, Z.F. Wang, K. Storr, L. Balicas, F. Liu, P.M. Ajayan, Nat. Mat. **9**(5), 430–435 (2010)
22. H. Nozaki, S. Itoh, J. Phys. Chem. Solids **57**, 41 (1996)
23. K. Yuge, Phys. RevB **79**, 144109 (2009)
24. I. Guilhon, M. Marques, L.K. Teles, F. Bechstedt, Phys. Rev. B **95**, 035407 (2017)
25. A. Jamróz, J.A. Majewski, Comput. Mater. Sci. **147**, 115–123 (2018)
26. R. D'Souza, S. Mukherjee, T. Saha-Dasgupta, J. Alloys Comp. **708**, 437–443 (2017)
27. A. Maity, S.J. Grenadier, J. Li, J.Y. Lin, H.X. Jiang, J. Appl. Phys. **123**, 044501 (2018)